Investigation of annealing-treatment on structural and optical properties of sol–gel-derived zinc oxide thin films

SHENGHONG YANG*, YING LIU, YUELI ZHANG and DANG MO

State Key Laboratory of Optoelectronic Materials and Technologies, School of Physics and Engineering, Sun Yat-Sen University, Guangzhou 510275, China

Abstract. The transparent ZnO thin films were prepared on Si(100) substrates by the sol–gel method. The structural and optical properties of ZnO thin films, submitted to an annealing treatment in the 400–700°C ranges are studied by X-ray diffraction (XRD) and UV-visible spectroscopic ellipsometry (SE). XRD measurements show that all the films are crystallized in the hexagonal wurtzite phase and present a random orientation. Three prominent peaks, corresponding to the (100) phase ($2\theta \approx 31\cdot8°$), (002) phase ($2\theta \approx 34\cdot5°$), and (110) phase ($2\theta \approx 36\cdot3°$) appear on the diffractograms. The crystallite size increases with increasing annealing temperature. These modifications influence the optical properties. The optical constants and thickness of the films have been determined by analysing the SE spectra. The optical bandgap has been determined from the extinction coefficient. We found that the refractive index and the extinction coefficient increase with increasing annealing temperature. The optical bandgap energy decreases with increasing annealing temperature. These mean that the optical quality of ZnO films is improved by annealing.

Keywords. ZnO films; SE spectra; optical constants; optical bandgap.

1. Introduction

Zinc oxide has many interesting optoelectronic properties such as a wide bandgap, a large exciton binding energy of 60 meV, and high transparency in the visible region. These properties have made way for many applications ranging from light emitting diodes, UV laser, transparent field effect transistors, solar cells and other optical coating applications (Natsume and Sakata 2000; Hoffman *et al* 2003; Osinsky *et al* 2004). Due to the various attractive properties for practical applications of ZnO films, there has been much attention paid on the fabrication of ZnO films in recent years. A variety of techniques have been employed to fabricate ZnO thin films such as pulsed laser deposition (Kang *et al* 2004), rf magnetron sputtering (Lee *et al* 2000), chemical vapour deposition (Fay *et al* 2005), spray pyrolysis (Romero *et al* 2004) and sol–gel process (Chen *et al* 2005; Logothetidis *et al* 2008; Xuea *et al* 2008). Despite the crystalline quality being inferior to other vacuum deposition techniques, the sol–gel processing still offers the possibility of preparing a small as well as large-area coating of ZnO thin films at low cost for technological applications. Even though there are earlier reports on the optical and structural properties of ZnO films deposited by sol–gel (Chen *et al* 2005; Logothetidis *et al* 2008; Xuea *et al* 2008), there are a few systematic studies on the effect of annealing on structural and optical properties, which are important parameters to be taken into consideration when we look for optoelectronic applications for these films. In this work, we deal with structural and optical properties of sol–gel derived ZnO thin films. As a consequence, the influence of annealing treatments on the structural and optical properties will also be investigated.

ZnO films were deposited at room temperature on Si (100) substrates by the sol–gel method. The key optical constants (refractive index, extinction coefficient) for the ZnO films were measured by spectroscopy ellipsometry (SE). SE is a non-destructive and sensitive optical technique that has been widely recognized as a reliable tool for characterizing optical properties of thin films (Azzam and Bashara 1977). In the analysis of the SE spectra, a four-phase model was employed, in which the optical properties of ZnO films were represented by the Forouhi-Bloomer (1986) model. Our main objective was to determine the optical properties of ZnO thin films as a function of annealing temperature.

2. Experimental

Figure 1 shows the flow chart of the preparation of the ZnO films. High-purity Zn-acetate dihydrate (Zn $(CH_3COO)_2\cdot2H_2O$, $99\cdot9\%$) was used as starting materials; methylglycol ($CH_3OCH_2CH_2OH$) was selected as a sol-

---

*Author for correspondence (shenghongyang@163.com)

vent, and diethanolamine ($C_4H_{11}NO_2$) was used as stabilizing agent. The concentration of zinc acetate was chosen to be 1 mol l^{-1}, and the resulting mixture was stirred for 1 h at 65°C, and then 3 h at room temperature to yield a clear and homogeneous solution, which served as the coating solution. The coating was usually made 3 days after the solution was prepared. The precursor solution was spun-coated onto Si(100) wafer for different measurements.

Spin coating was performed at room temperature, with a rate of 3000 rpm for 20 s and then of 5000 rpm for another 10 s. Si (100) substrates were ultrasonically cleaned with acetone and methanol, then etched for 1 min in 2% HF water solution in order to remove the surface oxide, followed by de-ionized water and dried in nitrogen before spin coating. After depositing by spin coating, the films were dried at 300°C for 10 min on a hotplate to evaporate the solvent and remove organic residuals. The procedures from coating to drying were repeated many times until the desired thickness of the films was reached. The films were then inserted into a furnace and annealed in air at 400–700°C for 2 h.

The film thickness was measured by profilometer (Dektak 3030). The crystal structure of the ZnO films was measured by using RIGAKU, D-MAX 2200 VPC X-ray diffractometer equipped with a Cu–Kα (λ = 1·540562 Å) source. The optical properties of the films were characterized by a high precision photometric ellip-

someter. Because the details on SE can be found in the literature (Azzam *et al* 1977), only a brief description is given here. In ellipsometry, the object is to measure the ratio of the complex Fresnel reflection coefficients, ρ, where

$$\rho = r_p/r_s = \tan\psi \exp(i\Delta). \tag{1}$$

The quantity, r_p (r_s), is the Fresnel reflection coefficients for light polarized parallel (perpendicular) to the plane of incidence, and ψ and Δ are the traditional ellipsometric angles. Note that both r_p and r_s contain information on the sample of optical and structural properties. The $\tan\psi$ and $\cos\Delta$ are measured in a photometric rotating-analyser ellipsometer, by Fourier analysis of curves of the light intensity vs the azimuthal angle of the rotating analyser. The SE measurements were carried out at room temperature in the 1·5–4·71 eV (corresponding to 263–827 nm) photo energy region at 0·03 eV intervals, operated at an angle of incidence of 70° and an azimuthal angle of the polarizer of 45°.

3. Results and discussion

Figure 2 shows X-ray diffraction patterns of ZnO thin films deposited on Si(100) substrate by spin-coating at different annealing temperatures of 400, 500, 600, and 700°C. At 400°C annealing, small peaks were observed and the film shows a poor crystallinity. Films annealed at temperature $\geq 500°C$, exhibit sharp diffraction peaks characteristics of the ZnO wurtzite. From figure 2, (100), (002), (101), (102), (110) and (103) XRD peaks were observed, and it is concluded that all the films were polycrystalline with a hexagonal wurtzite structure and a random orientation, which generally occurs in the growth of ZnO thin films (Xuea *et al* 2008). The degree of *c*-axis orientation of the ZnO thin films was strongly dependent
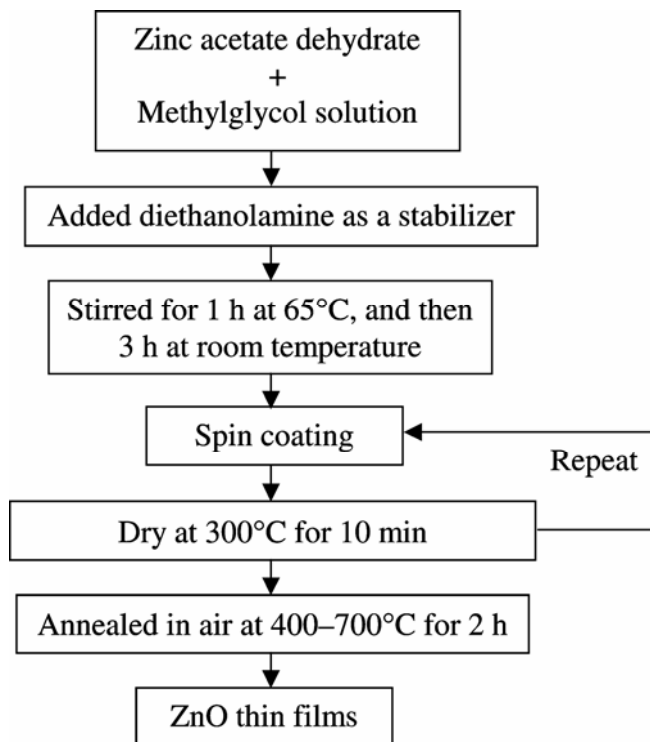

Figure 1. Flow chart for the preparation of ZnO thin film using sol–gel method.
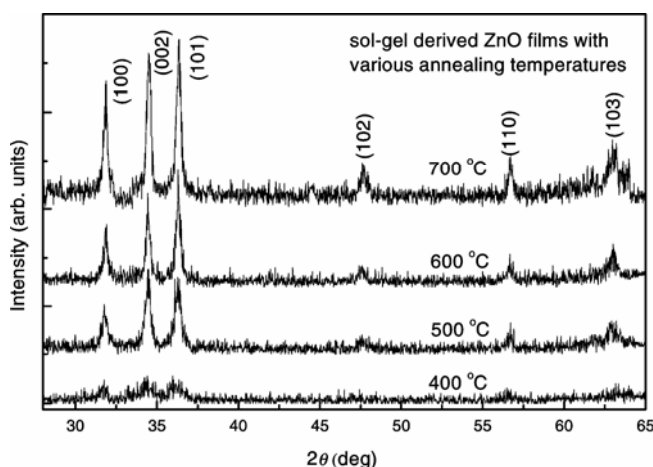
Figure 2. X-ray diffraction patterns of ZnO films with different annealing temperatures.

Table 1. List of samples studied.

ZnO annealing temperature	Determined by profilometer	Thickness (nm) Determined by SE	Particle sizes (nm)	E_g (eV)
400°C	192	190·2	–	3·405
500°C	173	170·8	24·15	3·360
600°C	163	166·1	33·74	3·354
700°C	155	154·2	34·36	3·343
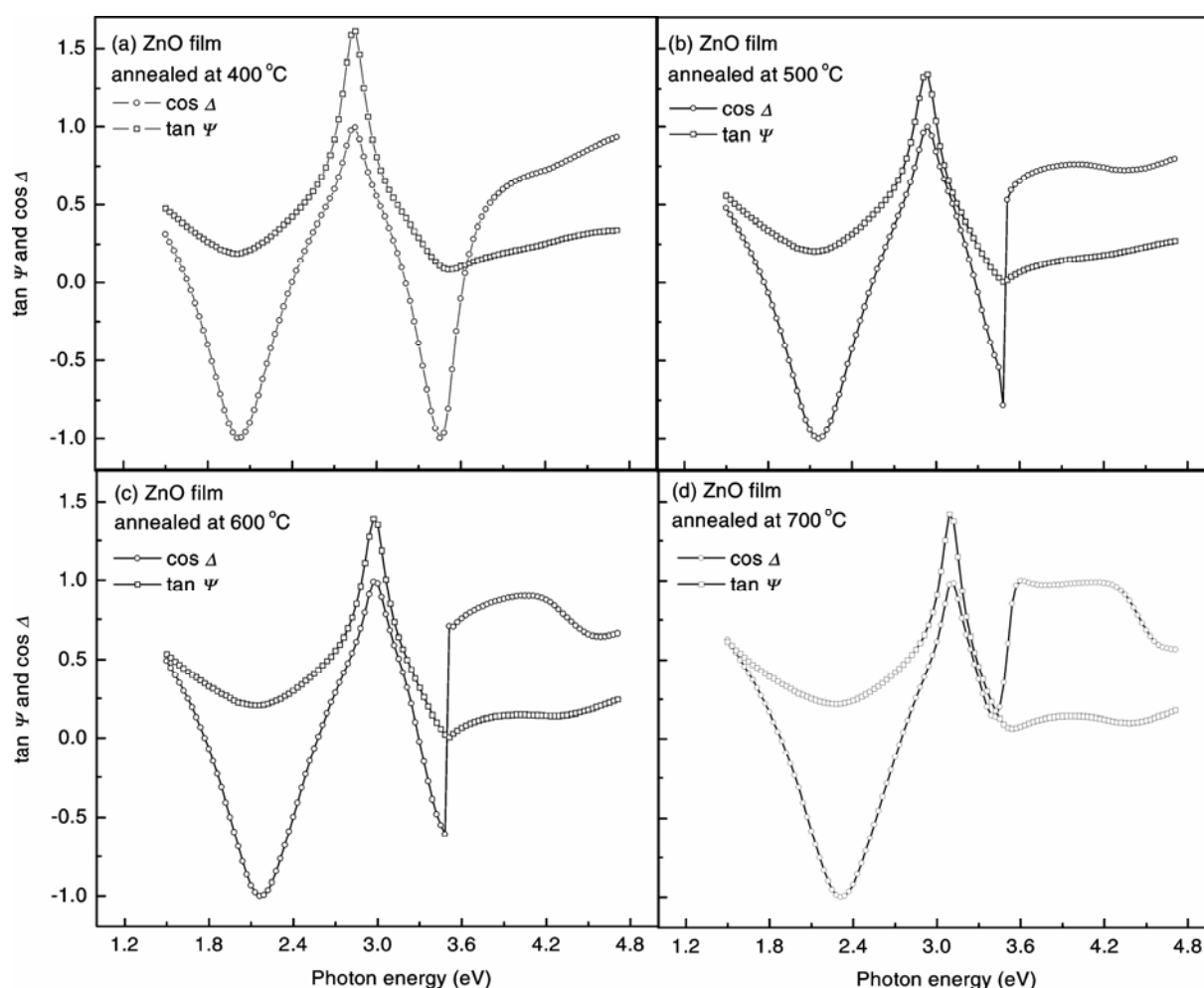
Figure 3. Experimental ellipsometric spectra of ZnO thin films with different annealing temperatures.

on the annealing temperature. It increases as the annealing temperature increases. The average ZnO thin film particle sizes were calculated using the full width at half maximum (FWHM) of (002) peak from the Scherrer's method and were presented in table 1. The calculated values of the crystallite sizes ranged between 20 and 40 nm. It was observed that crystallite size increased with increasing annealing temperature, which can be understood by considering the merging process induced from thermal annealing. For ZnO nanoparticles, there are many

dangling bonds related to the zinc of oxygen defects at the grain boundaries. As a result, these defects are favourable to the merging process to form larger ZnO grains while increasing the annealing temperature. The ZnO thin film thicknesses are also presented in table 1. It was observed that increasing the annealing temperature resulted in a decrease in film thickness from 190 nm (400°C annealing) to 154 nm (700°C annealing).

The FWHM of (002) plane of ZnO thin film with various annealing temperatures is also compared. As the anneal-

ing temperature increases from 400–700°C, the FWHM value exhibits a tendency to decrease, which can be attributed to the coalescences of grains at higher annealing temperature (Gupta and Mansingh 1996). As a result, it implies that the crystallinity of the ZnO thin films is improved at higher annealing temperatures. Other workers (Moustaghfir *et al* 2003; Kuo *et al* 2006) have also observed the improvement in crystallinity of the ZnO thin films with the increase of annealing temperature. These may be due to high annealing temperature providing energy to crystallites gaining enough energy to orient in proper equilibrium sites, resulting in the improvement of crystallinity and degree of orientation of the ZnO films.

The SE spectra for ZnO thin films annealed at various temperatures are shown in figures 3(a)–(d). The spectra can be separated into two spectral ranges. In the lower energy range, the spectra exhibit oscillations. This is only due to the interference effect of light, and this indicates that the films are transparent. The oscillating frequency depends on the thickness of the film. Generally, the thicker the film, the higher is the frequency. In the higher energy range, no interference oscillation is seen because of the occurrence of light absorption resulting from the interband transition in ZnO films.

The optical constants derived from the ellipsometric parameters of $\tan\psi$ and $\cos\Delta$ are analysed by a four-phase model (air/ZnO + voids/ZnO/substrate). The presence of a (ZnO + voids) layer is due to the surface roughness, which was modeled using a Bruggeman effective medium approximation (Bruggeman *et al* 1933) consisting of voids and ZnO. This feature is common for sol–gel-derived oxide thin films (Raham *et al* 1998). The optical constants of ZnO were parametrized using the Forouhi–Bloomer models, given by (Forouhi and Bloomer 1986)

$$n(E) = n_\infty + \frac{A\left(\begin{array}{c} -B^2E + 2DBE - 2D^2E + \\ 2CE + D^2B + BC - 4DC \end{array}\right)}{\sqrt{4C - B^2} \cdot (E^2 - BE + C)}, \quad (2)$$

$$k(E) = \frac{A(D - E)^2}{E^2 - BE + C}, \quad (3)$$

where E is the photon energy and the fitting parameters are A, B, C, D and n_∞. The optical constants of the substrate, Si(100), were taken from the work of Jellison (1992). With the help of simulated annealing optimization (Kirkpatrick *et al* 1983), the fitting parameters as well as the film thicknesses were determined by fitting the ellipsometric spectra. Figure 4 shows a fit for ZnO thin film annealed at a temperature of 700°C.

Clearly, the fit shown in figure 4 is a good fit. The thicknesses of ZnO films obtained by SE closely match with those obtained by profilometer (as shown in table 1). Therefore, it is verified that our model adequately describes the measured data. Figure 5 shows the refrac-

tive index (n) and extinction coefficient (k) obtained from the fitted parameters for ZnO thin films annealed at various temperatures. From figure 5, we find that the optical constants spectra of all ZnO films show a high refractive index ($n = 1\cdot8 \sim 2\cdot3$) in the UV-visible region as well as the fundamental absorption edge in the near ultraviolet region. The refractive index first increased and then decreased as the photon energy increased from 1·5 to 4·7 eV. The extinction coefficient of the films increases as photon energy increases, consistent with Kramers–Kronig relations. The extinction coefficients are very small at lower photon energy, where the films are nearly transparent. Our refractive index is smaller than the average value of ZnO bulk (refractive index ~ 2) in the visible wavelength range. This slight variation might be attributed to the porous nature of the sol–gel derived thin films. On the other hand, we also find different values of the refractive index and extinction coefficient due to the different annealing temperatures. The refractive index of the ZnO films increases with increasing annealing temperature. This conforms to the results already reported by Moustaghfir *et al* (2003). A higher annealing temperature enhances the formation of larger and more closely packed crystals. The increase of the refractive index with increasing annealing temperature can be partly attributed to improvement in film quality with the reduction in porosity in the ZnO film with annealing.

From the spectral relationship between extinction coefficient and photon energy (as shown in figure 5), the extinction coefficient of ZnO thin films can be divided into three regions: Region I having the low-energy regions ($E = 1\cdot5 \sim 2\cdot7$ eV, below the fundamental bandgap energy, E_g); regions II and III the high-energy regions ($E = 2\cdot7 \sim 3\cdot5$ and $3\cdot5 \sim 4\cdot7$ eV, above E_g). No obvious absorption is found below the fundamental bandgap
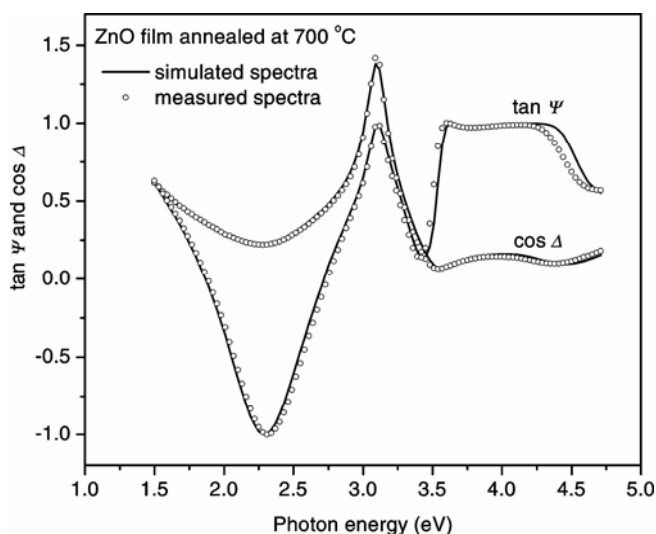
Figure 4. Experimental spectra (cycle) and calculated spectra (solid line) of ZnO thin films annealed at 700°C.

energy, E_g, so the extinction coefficient is zero except when the photon energy increased close to the bandgap energy. The dispersion in regions II and III are due to the transition from the valence band to the conduction band, or a transition from a band to an impurity level. It is interesting that the extinction coefficient increases as the annealing temperature also increases in regions II and III. The values of the extinction coefficient, as we know, result from the absorption and grain scattering when the photon wavelength is equivalent to the grain size in the high-energy region. The possibility of scattering of the grains increases as the annealing temperature increases, which can also be attributed to the increase of grain size and surface density of the films. The extinction coefficient near the fundamental bandgap energy is not zero because of the noise, and the results demonstrated that some other absorption is present in addition to the fundamental transition.

The optical bandgap energy, E_g, of ZnO films annealed at various temperatures were calculated by considering a direct allowed electronic transition between the highest occupied state of the valence band and the lowest occupied state of the conduction band when a photon of energy, $h\nu$, falls on the material. In this case, the absorption coefficient, α, is related to the optical bandgap energy, E_g, as (Tauc 1974)

$$(\alpha h\nu)^2 = \text{constant} \cdot (h\nu - E_g),\tag{4}$$

where

$$\alpha = 4\pi k/\lambda,\tag{5}$$

the E_g values are therefore determined by extrapolating the linear portion of the plot relating $(\alpha h\nu)^2$ vs $h\nu$ to $(\alpha h\nu)^2 = 0$. As an example, figure 6 shows the optical bandgap energy for ZnO thin film annealed at a temperature of 700°C, $E_g = 3\cdot343$ eV.

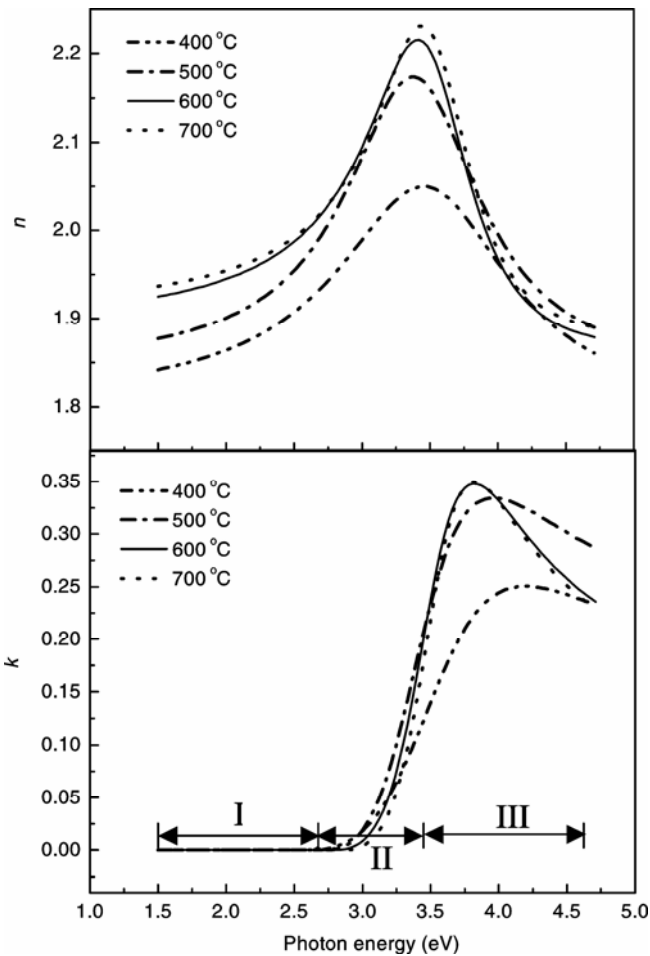Figure 7 shows the variation of E_g with annealing temperature. The E_g value is found to decrease from 3·405–
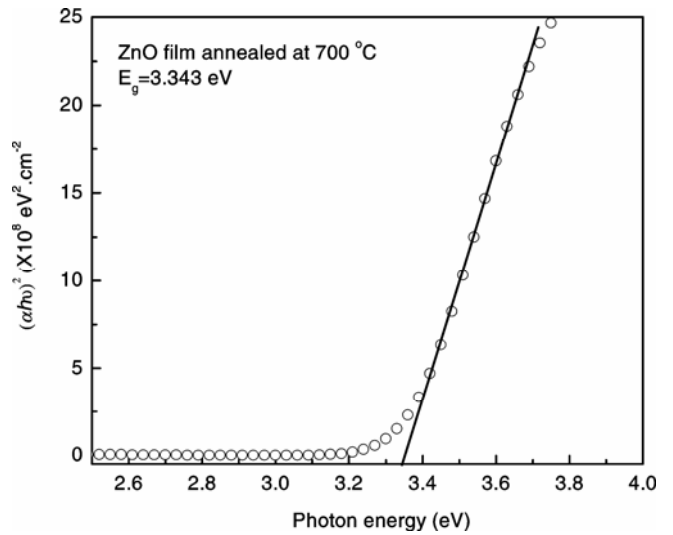

Figure 6. Plot of $(\alpha h\nu)^2$ versus $h\nu$ for ZnO thin films annealed at 700°C, the optical bandgap energy, E_g, is deduced from extrapolation of the straight line to $(\alpha h\nu)^2 = 0$.
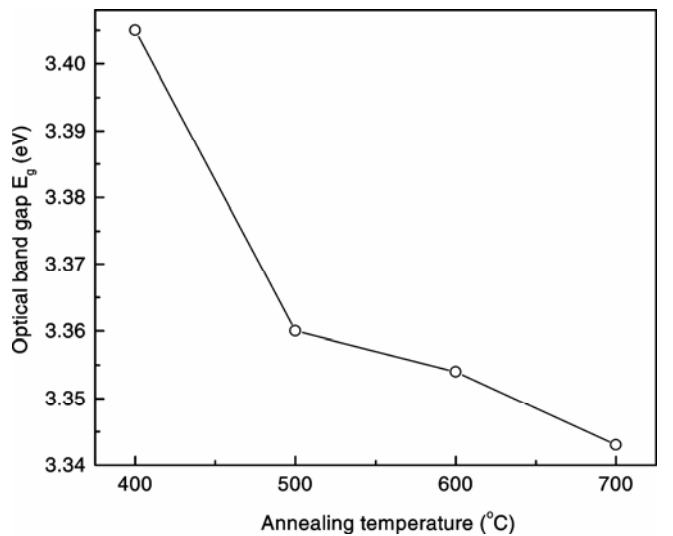

Figure 5. Optical constants (n and k) of ZnO thin films with different annealing temperatures.

Figure 7. Optical bandgap energies of ZnO films as a function of annealing temperature.

3·343 eV with increasing annealing temperature from 400–700°C. The decrease in E_g indicates an improvement of the quality of the film due to the annealing out of the structural defects. This is in agreement with the experimental results of XRD analysis. According to XRD results, the mean grain size increased with increased annealing temperature. As grain size increased, the grain boundary density of a film decreased, subsequently, the scattering of carriers at grain boundaries decreased (Lee *et al* 2003). A continuous increase of optical constants and also a shift in absorption edge to a higher wavelength with increasing annealing temperature may be attributed to the improvement in the crystalline quality of the films along with reduction in porosity.

The decrease in optical bandgap energy is generally observed in the annealed direct-transition-type semiconductor films. Hong *et al* (2005) observed an optical bandgap shift of ZnO thin films from 3·31–3·26 eV after annealing, and attributed this shift to the increase of the ZnO grain size. Chaparro *et al* (2000) ascribed this 'red shift' in the energy gap, E_g, to an increase in crystallite size for the annealed ZnSe films. Bao and Yao (2001) also reported a decrease in E_g with increasing annealing temperature for $SrTiO_3$ thin films, and suggested that a shift of the energy gap was mainly due to both the quantum-size effect and the existence of an amorphous phase in thin films. In our case, the mean crystallite size increases from 20 to 40 nm after annealing from 400–700°C. Moreover, it is understood that the amorphous phase is reduced with increasing annealing temperature, since more energy is supplied for crystallite growth, thus resulting in an improvement in crystallinity of the ZnO films. Therefore, it is believed that both the increase in crystallite size and the reduction in amorphous phase amount are responsible for the bandgap decreasing in annealed ZnO films. The change of refractive index, n, extinction coefficient, k, and optical bandgap energy, E_g, reveals the impact on optical properties of thermal treatment.

4. Conclusions

The effect of post-annealing treatment on structural and optical properties has been critically examined in sol–gel derived ZnO films on Si(100) by XRD and SE in the UV-visible region. XRD spectra and refractive index of the films reveal that the crystalline nature of the films has significantly improved with annealing. The optical constants and optical bandgap energy of ZnO films were dependent on the annealing temperature. The thickness values obtained from SE measurement compare well with the surface profilometer data. The refractive index for ZnO films increases as the annealing temperature is increased. The optical bandgap energies have been found to decrease from 3·405 to 3·343 eV as annealing temperature is increased from 400–700°C. These optical property modifications can be attributed to structural modifications with different annealing temperatures.

References

Azzam R M A and Bashara N M 1977 *Ellipsometry and polarized light* (Amsterdam: North-Holland) p. 89
Bao D and Yao X 2001 *Appl. Phys. Lett.* **79** 3767
Bruggeman D A G 1933 *Ann. Phys. Leipzig* **24** 636
Chaparro A M, Martinez M A, Guillen C, Bayon R, Gutierrez M T and Herrero J 2000 *Thin Solid Films* **361** 177
Chen S Q, Zhang J and Feng X 2005 *Appl. Surf. Sci.* **241** 384
Fay S, Kroll U and Bucher C 2005 *Sol. Energy Mater. Sol. Cells* **86** 385
Forouhi A R and Bloomer I 1986 *Phys. Rev.* **B34** 7018
Gupta V and Mansingh A 1996 *J. Appl. Phys.* **80** 1063
Hoffman R L, Norris B J and Wager J F 2003 *Appl. Phys. Lett.* **82** 733
Hong R, Huang J, He H, Fan Z and Shao J 2005 *Appl. Surf. Sci.* **242** 346
Jellison Jr. G E 1992 *Opt. Mater.* **1** 41
Kang H S, Kang J S, Kim J W and Lee S Y 2004 *J. Appl. Phys.* **95** 1246
Kirkpatrick S, Gelatt C D and Vecchi M P 1983 *Science* **220** 671
Kuo S Y, Chen W C and Cheng C P 2006 *Superlattices and Microstr.* **39** 162
Lee J C, Kang K H and Kim S K 2000 *Sol. Energy Mater. Sol. Cells* **64** 185
Lee J H, Ko K H and Park B O 2003 *J. Cryst. Growth* **247** 119
Logothetidis S, Laskarakis A, Kassavetis S, Lousinian S, Gravalidis C and Kiriakidis G 2008 *Thin Solid Films* **516** 1345
Moustaghfir A, Tomasella E, Ben Amor S, Jacquet M, Cellier J and Sauvage T 2003 *Surf. Coat. Technol.* **174/175** 193
Natsume Y and Sakata H 2000 *Thin Solid Films* **372** 30
Osinsky A, Dong J W, Kauser M Z, Hertog B, Dabiran A M and Chow P P 2004 *Appl. Phys. Lett.* **85** 4272
Raham M M, Yu G L, Krishna K M, Soga T, Wantanable J J, Jimbo T and Umeno M 1998 *Appl. Opt.* **37** 691
Romero R, Lopez M C and Leinen D 2004 *Mater. Sci. Eng.* **B110** 87
Tauc J C 1974 *Amorphous and liquid semiconductor* (New York: Plenum Press) p. 159
Xuea S W, Zu X T, Zhouc W L, Denga H X, Xiang X, Zhang L and Dengd H 2008 *J. Alloys Compds.* **448** 21